THE JOURNAL OF PHYSICAL CHEMISTRY C
A JOURNAL OF THE AMERICAN CHEMICAL SOCIETY

pubs.acs.org/JPCC
Article

Up-Converting Luminescent Nanoparticles as Probes of Surface Dynamics in Single Evaporating Microdroplets of Suspension

Yaroslav Shopa, Maciej Kolwas, Daniel Jakubczyk,* Gennadiy Derkachov, Izabela Kamińska, Krzysztof Fronc, and Tomasz Wojciechowski

Cite This: J. Phys. Chem. C 2025, 129, 8955−8965
Read Online
ACCESS | Metrics & More | Article Recommendations

ABSTRACT: We have investigated the optically measurable properties of single evaporating microdroplets of suspensions containing up-converting luminescent nanoparticles (Gd_2O_3:Er^{3+}), levitated in a linear electrodynamic trap. These microdroplets served as spherical optical cavities, with their resonance properties influenced by the distribution and interactions of nanoparticles (NPs), acting as nanoprobes. Using a combination of light scattering theories, we examined the evolution of the microdroplet radius, nanoparticle surface organization, and effective refractive index during evaporation. Up-conversion luminescence, driven by 805 nm excitation, enhanced the resolution of these observations. Key findings reveal that the increasing NP density in the surface layer leads to surface saturation, followed by transitions to a gel-like state through successive layer formation and collapse. Scattering and luminescence signals exhibit complex oscillatory behaviors linked to resonance phenomena and nanoparticle migration driven by photophoretic forces. Theoretical modeling closely aligns with experimental trends, confirming the interplay between the NP distribution and optical resonance properties.

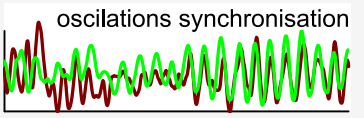

1. INTRODUCTION

Evaporating microdroplets of colloidal suspension represent complex microsystems, whose physical and optical properties evolve dynamically over time. As they dry, these droplets undergo changes in size and shape, accompanied by internal rearrangements of suspended particles that profoundly influence their optical characteristics. Understanding this evaporation process is crucial across disciplines such as materials science,[1] medical science,[2] and climate modeling.[3,4] Evaporation is a scientifically important, inherently complex process,[5,6] which can provide a practical method for creating functional nanomaterials utilized in sensors, optical, and biological devices.[7]

Of particular interest are optical cavity resonances, known as Morphology Dependent Resonances (MDRs), or, in certain cases, Whispering Gallery Modes—arising naturally from light confinement within spherical geometries.[8,9] These modes are sensitive to subtle changes in droplet size, shape, and refractive index distribution—affected, for example, by the arrangement of suspended nanoparticles—thus offering unique insights into both surface and internal processes within the droplet.[10,11]

The use of nanoparticles as optical nanoprobes is well-established (see, e.g., refs [12,13] for reviews), with luminescent nanoparticles significantly enhancing observational resolution.[14] Further enhancement appears achievable through the utilization of up-converted luminescence.

Observed oscillations of luminescence and scattered light in drying droplets reveal intriguing optical properties. Typically, luminescence and scattering oscillations share the same frequency and phase, highlighting their common resonant origin: a strong inducing light field. However, instances of differing frequencies suggest that these phenomena may be induced by distinct cavity modes within the droplet, underscoring complex mode interactions and sensitivity to internal structural changes.

In this study, we investigate the interplay between nanoparticle distribution dynamics—driven by evaporation and photophoretic forces—and the evolution of optical cavity resonances within drying droplets.

We present detailed experimental analyses and spectral data demonstrating that optical cavity modes act as highly sensitive indicators of nanoparticle spatial rearrangements and droplet evaporation dynamics. By examining the evolution of spectra as droplets dry, particularly the cavity resonances they exhibit, we gain insights into the changing nanoparticle distributions.

Our findings provide new optical methods for probing internal droplet states, with potential applications ranging from environmental monitoring—such as aerosol characterization and understanding atmospheric droplet interactions[15−17]—to technological fields, including controlled drying processes and microfluidic diagnostics.

Received: January 9, 2025
Revised: April 7, 2025
Accepted: April 10, 2025
Published: May 1, 2025

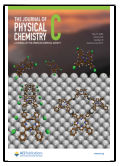

https://doi.org/10.1021/acs.jpcc.5c00174
J. Phys. Chem. C 2025, 129, 8955−8965

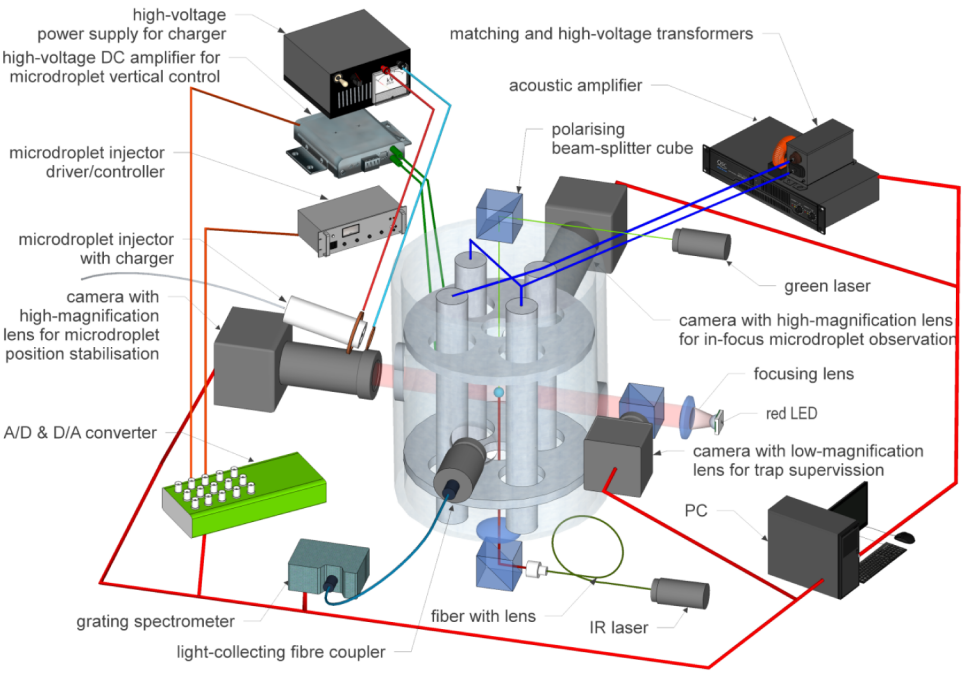

Figure 1. Schematic diagram of the experimental setup.

2. EXPERIMENTAL SETUP AND METHODS

As presented in Figure 1, the experiments were conducted in an in-lab-built linear electrodynamic quadrupole trap (LEQT; compare refs [18−20]). The essential trap configuration was the same as previously described in ref 14, so only the introduced improvements will be discussed in greater detail. Electrically charged droplets were confined horizontally with the quadrupolar AC field generated by rod electrodes, while vertical confinement was achieved with the DC field of the plate electrodes. The field between the plate electrodes, in the configuration we used, is not homogeneous around the center of the trap but exhibits a gradient, which enables the translation of microdroplets vertically by varying the applied voltage. The levitating microdroplet was backlit with a bright red LED, and its (vertical) position was observed as a shadow with a digital camera (Smartek, GC651MP, equipped with IR filters) through a high-magnification microscope at 10 fps, with a resolution of ∼1.0 μm/pixel. It enabled microdroplet radius measurement (shadowgraphy) as well as the set up of a stabilization loop to keep the droplet at the desired vertical location—on the (horizontal) axis of the light-collecting optics.

Two types of nanoparticles were used: Gd_2O_3:6%Er^{3+} 353 nm diameter, and Gd_2O_3:8%Er^{3+} 126 nm diameter. Both were suspended in DEG by mixing the dry powder and sonication for several hours until no sediment was present. The mass concentration of NPs was 5 mg/mL, on loading the suspension to the injector. Since the density of Gd_2O_3 (∼7.1 g/cm^3) is very high in comparison to that of DEG (∼1.1 g/cm^3), the viscosity of DEG (∼37 mPa·s) is not high enough to suppress sedimentation. Thus, the initial mass concentration of NPs in the microdroplet, w_{NP}, could be slightly different (usually lower). When the suspension was stored, it was kept in a refrigerator at ∼8 °C in a vertical tube rotator. It was then sonicated for 2−3 h before the experiments, which were conducted immediately afterward. The in-lab synthesis of Gd_2O_3:Er^{3+} was described in refs 14 and 21.

Microdroplets were delivered to the trap with an in-lab-built droplet-on-demand piezoelectric injector equipped at the nozzle with annular electrodes for droplet charging,[18] compare e.g., ref 22 The high voltage used for charging was switched on only during droplet injection and turned off directly afterward in order to avoid influencing the trapping field during the stabilizing loop operation. In spite of significant effort, due to some sedimentation in the injector, the parameters of the microdroplets (radius, charge, and initial NS number concentration) varied noticeably, though not significantly.

In this set of measurements, the microdroplet was illuminated with an IR beam from below to counteract possible sedimentation of Gd_2O_3 nanoparticles in the microdroplet. In order to circularize the beam and, most of all, suppress the spatial fringes produced by the multijunction laser diode, the beam was passed through the multimode 200 μm fiber. The spatial mode structure inherited from the fiber turned out to be much less harmful to the repeatability of the experiment.

The scattered light and luminescence were collected with a dedicated objective and fed to a small grating spectrometer (USB4000, Ocean Optics) via a 400 μm fiber. We observed the scattering of laser light at wavelengths of 805 nm (attenuated with two OD6 notch filters) and 515 nm, as well as up-converted luminescence induced by 805 nm radiation, detected at several lines within two bands: red and green—see Figure 2. Due to the low luminescence light intensity, the integration time had to be set to ∼1 s. This set the limit to the temporal resolution of the experiments. All measurements were performed under ambient conditions, while the lab was air-conditioned with the temperature set at 22 °C.

The experimental data (including the spectra) can be accessed at the data repository,[23] particularly samples DI192: experiments 003 and 006, which we discuss below, and sample DI216—experiment 029, which was used to detect photophoretic forces within the microdroplet.

https://doi.org/10.1021/acs.jpcc.5c00174
J. Phys. Chem. C 2025, 129, 8955−8965

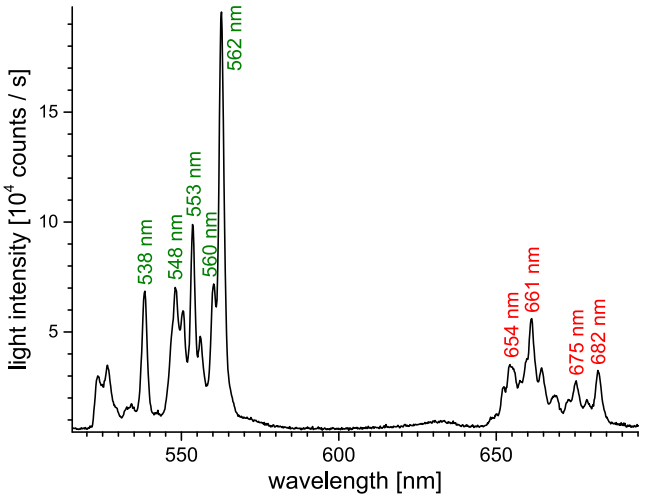

Figure 2. A fragment of the spectrum—green and red luminescence bands—observed for a microdroplet of 55-μm diameter containing Gd_2O_3:6%Er^{3+} nanoparticles of 508 nm diameter (~40 mg/mL in triethylene glycol). The temporal evolution of the marked lines was followed.

3. RESULTS AND DISCUSSION

3.1. Microdroplet Radius Evolution as a Probe of System Dynamics. As we have shown in our previous works (see, e.g., refs 24 and 25 , several conclusions can be drawn solely by analyzing the droplet evaporation rate. Indeed, the studied microdroplets exhibited some meaningful departure of radius evolution from the so-called radius-square-law, as shown in Figure 3a,b for two different droplets (experiments 003 and 006, respectively, as declared in Section 2). The departure can be observed both for the smaller droplet exhibiting a significant, over 3.2:1, radius change (Figure 3a), and for the larger droplet with only 1.2:1 radius change (Figure 3b). The evaporation rate of both droplets (radius change rate, dR/dt) increases, though at different paces, marked by inflection points and "kinks." However, only for the smaller droplet (Figure 3a), the rate suddenly decreases and stabilizes at a significantly lower magnitude of ~5600 s.

It is known that the evaporation rate depends on the energy balance in and around the droplet, as well as on the composition (molar fractions) on both sides of the gas−liquid interface (see, e.g., refs 26 or 27 . We have verified, by changing the 805 nm laser power, that the dR/dt increase is due to the warming of the droplet caused by radiation absorption in NPs. Since the number of NPs in the droplet is constant (the same power is absorbed), while the volume of the host liquid is decreasing, the evaporation rate is expected to increase, which we generally observe. On the other hand, the change in droplet composition can slow the evaporation down. It can be intuitively understood that, since evaporation occurs only from the open liquid surface, solid particles present at the interface reduce the area available for evaporation, effectively "clogging" the interface. This is expected to happen around 5600 s in Figure 3a, where the entire droplet becomes a wet aggregate of NPs, which then dries very slowly (compare ref 28). Since the used NPs are wettable with DEG, they tend to stay slightly under the surface until they all get in contact due to the droplet evaporation—and hence a rapid transition in the evaporation rate. The mass of the final aggregate of NPs (estimated from the observed radius and assumed NPs filling factor of 0.74) was found to be consistent with the initial suspension concentration, so it is understood that no significant voids formed in the final aggregate of NPs.

It can be readily noticed that the above reasoning cannot explain all of the aforementioned "kinks" in dR/dt. Such rapid changes are not predictable with the effective medium approach and require considering equally rapid changes in the NPs' ordering—structural changes of the microdroplet—perhaps forming transient surface layer(s) of NPs, as we considered in refs 10 and 29. We will try to elucidate this by studying light scattering from the composite droplet and luminescence from the NPs within it.

3.2. Internal Light Distribution and Far-Field Scattering as Potential Probes of a Composite Microdroplet Structure. It has long been established that light scattering patterns from a pure liquid droplet can be quite accurately

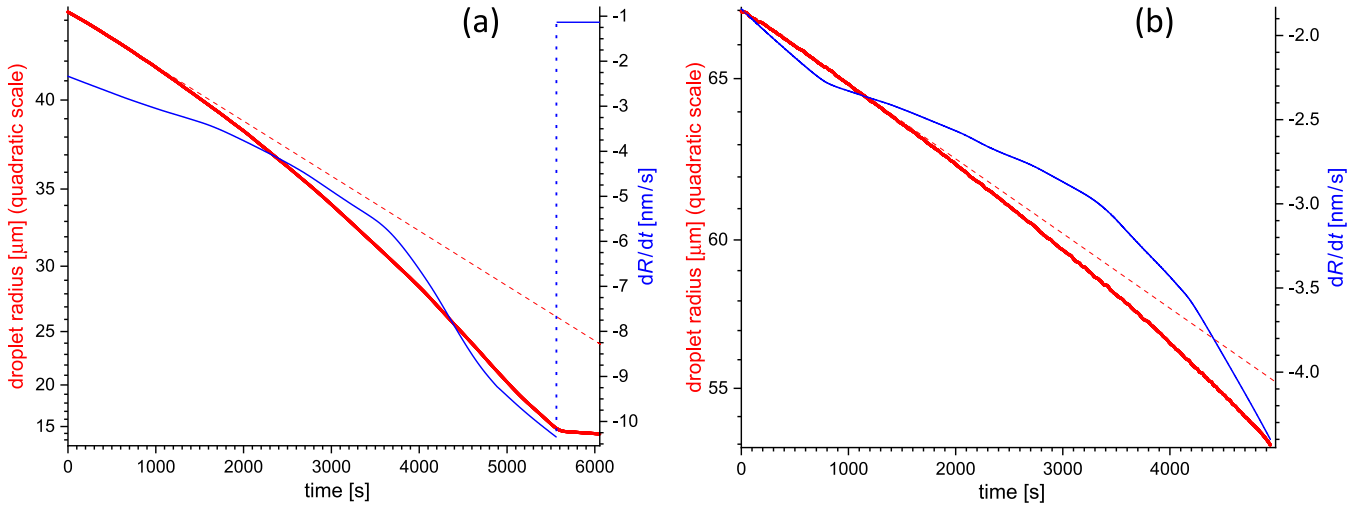

Figure 3. Evolution of the microdroplet radius R (smoothed using Lowess with a 131-point window) and the corresponding radius change rate dR/dt (smoothed using Lowess with an 899-point window) for two microdroplets in different size ranges: (a) 44−14 μm and (b) 67−53 μm. The vertical axes are on quadratic scales, so evaporation following the radius-square law should appear as a straight line, indicated by the red dashed lines.

https://doi.org/10.1021/acs.jpcc.5c00174
J. Phys. Chem. C 2025, 129, 8955−8965

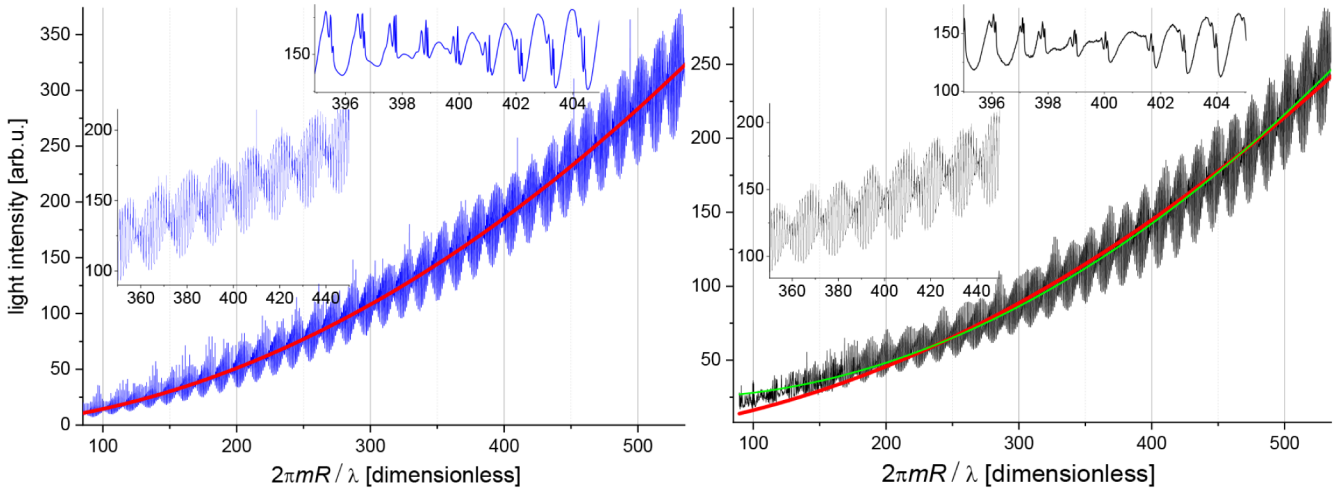

Figure 4. Scattered light intensity in the far field, integrated over the field-of-view of $(90 \pm 16° \times 0 \pm 5°)$. Left panel: Mie theory calculation. Right panel: experiment was done on a pure DEG microdroplet. For both panels: wavelength λ = 458 nm, refractive index of DEG at 22 °C and 458 nm, m = 1.4524. The radius-square law is shown as a red solid line in both panels. The experimental intensity trend (green solid line) deviates slightly from the radius-square law due to limited purity (99.9%) of DEG used in the experiment.

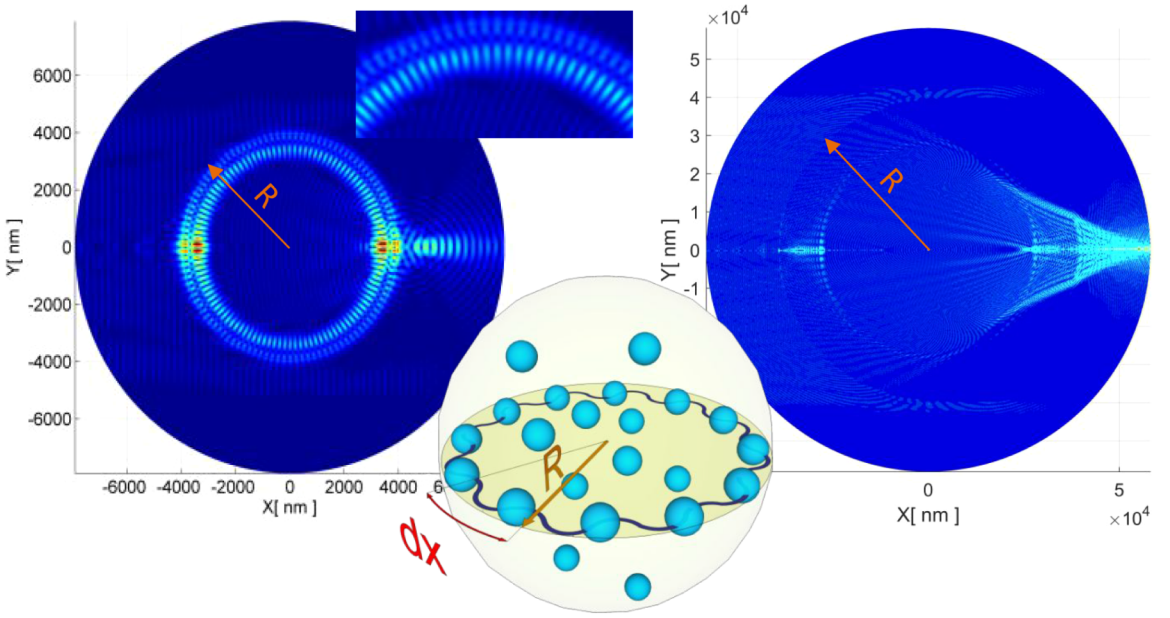

Figure 5. Left and right panels: light intensity distribution in the equatorial plane cross-section, as predicted by Mie theory for a homogeneous sphere with the refractive index m = 1.45. The sphere is illuminated by a plane wave from the left. The distributions of both internal and near-field intensities is visible. Left panel: at a narrow resonance, showing a characteristic mode structure—a standing wave—is seen for the droplet radius R = 3953 nm and wavelength λ = 532.07 nm, with a magnified fragment ($X \in [-2000, 2000]$, $Y \in [2000, 4000]$) shown in the top inset. Right panel: R = 38768 nm, λ = 805 nm—typical out-of-resonance case. Bottom inset: conceptualization of a microdroplet of nanoparticle suspension, with a standing light wave interacting with the nanoparticles in the equatorial plane.

reproduced using Mie theory,[30] as demonstrated in Figure 4, which shows far-field light scattering intensity during the evaporation of a single diethylene glycol droplet. The main limitation to this accuracy arises from deviations in the droplet's sphericity, where even minor discrepancies affect the structure of narrow MDRs, as visible in the figure. The time-averaged intensity of light scattered by a spherical object is proportional to its surface area, as indicated by the red lines in Figure 4 (compare, e.g., ref 24—this "radius-square" law is quite robust). The scattered light intensity also exhibits modulation versus the droplet radius due to spherical cavity modes. The amplitude of this modulation, which constitutes only a small fraction of the total scattered light intensity, is itself proportional to the droplet's surface area.

On the other hand, for inhomogeneous droplets, the maxima observed in the scattered light intensity—associated with MDRs—cannot be explained by Mie theory alone. Here, we propose a combination of established methods to address this challenge.

Having measured the droplet radius, we calculated the scattered and internal light intensity distribution using Mie theory with the effective medium approximation, further incorporating the theory of light scattering by fractal aggregates (see, e.g., ref 31). In this way, we were able to verify the

https://doi.org/10.1021/acs.jpcc.5c00174
J. Phys. Chem. C 2025, 129, 8955−8965

hypothesis regarding the evolution of the NP distribution. Furthermore, by analyzing the evolution of luminescence signals—driven by the internal light intensity distribution evolution—we examined modifications to the resonance properties of the microdroplet, an inhomogeneous spherical optical cavity, altered or introduced by nanoparticles (NPs) and their distribution. In the following sections, we provide details of our analysis.

3.3. Intracavity Field Distribution versus NP Distribution and Migration. The scattered light intensity maxima observed in the far-field versus the size parameter for a homogeneous microsphere with a linear refractive index correspond to resonances of its internal field (see Figure 7 in ref 14, compare e.g., ref 32). This internal radiation intensity can be rigorously determined using Mie theory (see, e.g., refs [30,33]). It exhibits spatial modulation along the circumference of the droplet and tends to concentrate near the interface. The effect is particularly strong at resonances—see Figure 5 (compare e.g., refs [34,35]). However, for a spherical microdroplet containing a suspension of luminescent (nano)particles that absorb and scatter light, this provides only a rough approximation. Some phenomena can be grasped with an effective medium approach—as we show below—while an exact solution to the problem remains out of reach for now. However, to grasp/visualize the resonance properties of a spherical cavity, it turns out to be sufficient to consider a 2D model of a circular resonator[36]—see bottom inset in Figure 5. Thus, the intensity of radiation (light) at the circumference of a spherical cavity (homogeneous droplet) in the equatorial plane can be simplistically described as an intracavity standing wave:

$$I(R, x) \sim 1 + \cos(\Omega_R R)\cos(\Omega_x x) \tag{1}$$

where R is the droplet radius decreasing in time and x is the position along the circumference. This gives an intuitive picture of a complex distribution. The frequencies Ω_R and Ω_x can be determined by considering the interval/spacing between the consecutive intensity maxima/minima versus R and x: $dR = \lambda/2\pi m$ and $dx = \lambda/m$, where λ is the vacuum wavelength of radiation and m is the refractive index of the droplet. The obvious condition: $\Omega_x dx = \Omega_R dR = 2\pi$ leads to $\Omega_R = 4\pi^2\lambda/m dR = 2\pi\Omega_x$. Any phase relations are not of importance in this description.

As mentioned before, NPs dispersed in a microdroplet interact with its internal field (absorb and scatter), thus modifying it. In the modeling of scattering/absorption/luminescence on a microdroplet as a whole, the distribution of NPs—particularly near the surface, where the field is strongest at resonance—must be taken into account in some way and therefore must also be modeled/predicted beforehand.

Since the NP dispersion is usually charge-stabilized, their distribution naturally evolves from completely random to somewhat organized (e.g., hexagonal in layers), particularly at higher NP number densities. We assume that the NP distribution in the microdroplet surface layer (most important for interactions with radiation) can be approximated as Gaussian, characterized by the mean distance μ and standard deviation σ (distribution width):

$$N(x) = \frac{N_{surf}}{\sigma\sqrt{2\pi}}\exp\left[-\left(\frac{x-\mu}{\sqrt{2}\sigma}\right)^2\right] \tag{2}$$

where N_{surf} is the number of NPs in the surface layer and σ is obviously much smaller than the droplet circumference $2\pi R$. When NPs arrange themselves in a regular pattern—transitioning from a "surface gas" to a "surface solid" phase, σ becomes smaller.

As mentioned above, just after droplet formation, at the beginning of the evolution, the number density n of NPs in the droplet can be considered uniform—equal at the surface and in the droplet volume $n_{surf} = n$. Due to the evaporation of the dispersion medium, the droplet surface moves radially and captures particles from the evaporated volume. Additionally, the existence of surface adsorption and the charge of NPs helps to move them to the interface until all radial forces acting on the NPs are equilibrated[37] and most of the nanoparticles reside at or close to the interface. The details of the evolution depend on the relationship among the mentioned processes. In this consideration, N_{surf} was simplistically modeled as resulting only from droplet evaporation—interface inward movement:

$$N_{surf}(R) \cong \frac{w_{NP}(R_0^3 - R^3)}{\rho_{NP} r^3} \tag{3}$$

where R_0 is the initial droplet radius, w_{NP} is the initial mass concentration of NPs, r is the NP radius, and ρ_{NP} is the density of the NPs' material. This formula should reasonably describe the number of NPs at the surface until surface saturation, while after surface collapse(s), it should give the total number of NPs in the near-interface layers. We shall verify this assumption in Section 3.4.2.

On the other hand, light-absorbing NPs are expected to migrate to the minima of absorbed light intensity due to photophoretic forces, rather than to the maxima via gradient forces, thereby reflecting the temporal evolution of these minima. We verified this in a separate experiment in which the intensity of 805 nm radiation was modulated—see Figure 6. It can be observed that the luminescence signal closely follows the excitation, represented by scattering at the same wavelength, while scattering at a different wavelength (515 nm) is nearly in counter-phase. As can be readily inferred from the

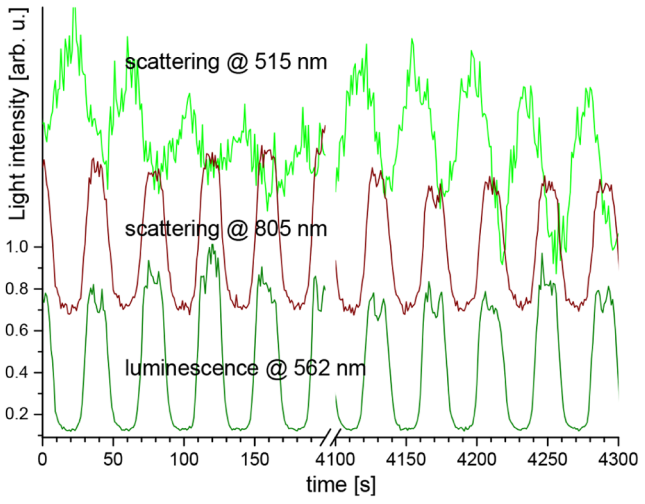

Figure 6. Scattering of light from, and luminescence emitted by, an evaporating droplet of a suspension containing luminescent nanoparticles (NPs). The ordinate scale for each signal is independent and presented in arbitrary units. The beginning and end of the droplet's evolution are shown.

https://doi.org/10.1021/acs.jpcc.5c00174
J. Phys. Chem. C 2025, 129, 8955−8965

right panel of Figure 5, the general distribution of bright and dark regions in the illuminated droplet does not vary significantly with wavelength when out of resonance (which is the case most of the time). This means that NPs driven toward darker regions by the photophoretic force due to 805 nm radiation also scatter less of the 515 nm radiation. Naturally, this effect is not present in the luminescence. A slight lag behind perfect counter-phase behavior is to be expected due to the effective viscosity of the suspension droplet. It is also reasonable to expect that NP migration is mostly local—that is, toward nearby field nodes.

Thus, it is expected that in the discussed experiments, the 805 nm radiation absorbed in Gd_2O_3:Er^{3+} NPs drives a "standing wave" of NPs density, which feedbacks with 805 nm internal field distribution and heavily influences scattering and luminescence at all wavelengths. Furthermore, this "standing wave" of NPs density modifies resonance properties to the microdroplet—introduces additional resonances and modifies the existing ones (compare e.g. refs [38,39]). We discuss this below in detail.

3.4. Scattering of Light on a Microdroplet of Suspension. Having in mind the considerations of the previous section, several hypotheses were tested using Mie theory-based codes, and we found that the increase in the effective refractive index of the microdroplet can explain the observed trend (long-time average) of the scattered light intensity (see the cyan line in Figure 7), but not the oscillatory

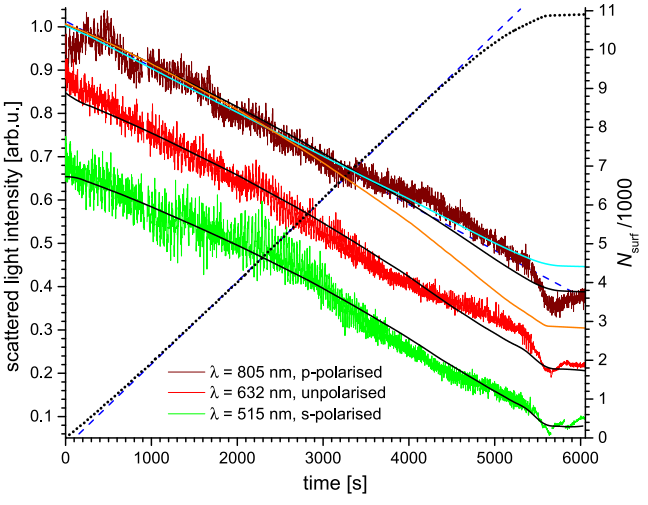

Figure 7. Scattered light intensity at three different wavelengths and polarizations. This incident light also differs in character: only 805 nm light is absorbed in NPs; 632 nm light is noncoherent. The scale for each trace is independent. The solid black lines are long-time averages predicted with eq 7. The orange and cyan lines correspond to $R(t)^2$ and the first term of eq 7, respectively. The dotted black line shows the predicted/modeled evolution of N_s. The dashed blue lines.

properties of the signal. A separate term describing the scattering on NPs is necessary. Using the analysis for the corresponding characteristic size relationship (spatial coherence criterion), presented e.g., in ref 31 , we have arrived at conclusion that the scattering on NPs is proportional to the number of NPs at the surface and must also depend on their distribution $N(x)$. In order to fully explain the oscillatory properties of the signal, the second term must be modulated by the internal field of the droplet. (we shall discuss the modulation of scattering and luminescence signals in detail in Section 3.4.3). Furthermore, the correlation between $N(x)$ and $I(x)$ should be accounted for. Thus, the intensity of light of wavelength λ, scattered on a microdroplet of radius R could be postulated as

$$I_{sca}(\lambda, R) \cong I_{eff}(\lambda, R, m_{eff}(R)) + \alpha \int_0^{2\pi R} N(R, x)\, I(R, x)\mathrm{d}x \quad (4)$$

where the proportionality factor α depends, among other factors, on the microdroplet and NP size parameter, and the composite microdroplet mass and surface fractal dimensions. I_{eff} is the intensity of light scattered by an effective homogeneous sphere with an effective refractive index m_{eff}, which follows a simple mixing rule for refractive indices of Gd_2O_3 and DEG:

$$m_{eff}(R) = c_{Gd_2O_3} \cdot m_{Gd_2O_3} + (1 - c_{Gd_2O_3}) \cdot m_{DEG} \quad (5)$$

where, in turn, $c_{Gd_2O_3}$ is the volume fraction of NPs residing in the near-surface layer of the droplet:

$$c_{Gd_2O_3} = r^2 N_{surf} / 4R^2 \quad (6)$$

The black dotted line in Figure 7 represents N_{surf} corresponding to the radius evolution shown in Figure 3a. The required change in the refractive index actually occurs in the near-surface layer of the droplet due to the accumulation of NPs there, which is the result of liquid evaporation. The value of the refractive index of the droplet interior was found to be less important, if not entirely negligible.

3.4.1. Scattering Long-Time Trend. It could be expected that the intensity of scattered light—its long-time trend—decreases in a similar manner as the square of the radius, as shown by the orange solid line in Figure 7 (compare Figure 3a). However, this is not the case, and the observed decrease resembles linear—see the blue dashed line in this figure. This is in line with what has been observed for the oscillatory part of the signal—see below—it indicates that there is a process that slows the evaporation down. As has been established, it is the presence of the suspended phase—NPs—that governs the phenomenon. NPs located in regions of a strong field (e.g., close to the surface) are expected to contribute the most to total scattering. It turns out that the averaged eq 7 predicts the observed trends quite well, as can be seen in Figure 7.

3.4.2. Impact of Photophoretic Force–Driven Nanoparticle Redistribution on Far-Field Scattering. Now, it must be noted that the second term in eq 4 does not hold well when $N(R,x)$ is itself driven by the strong internal field at the 805 nm line. In that case, we postulate a semiempirical formula:

$$I_{sca}(\lambda, R) \cong I_{eff}(\lambda, R, m_{eff}(R)) + \alpha N_{surf} I_{eff}(805, R + \beta {N_{surf}}^2, m_{eff}(R)) \quad (7)$$

which we will discuss in detail in the following sections. Again, the proportionality factors α and β depend, among others, on the microdroplet and NP size parameters, as well as the composite microdroplet mass and surface fractal dimensions. The factors we found for scattering at different wavelengths were consistent.

First of all, at this point, it is possible to verify the hypothesis on the $N_{surf}(R)$ evolution (eq 3). If we neglect the influence of the refractive index change/evolution and assume the long-

https://doi.org/10.1021/acs.jpcc.5c00174
J. Phys. Chem. C 2025, 129, 8955−8965

term trend of $I_{eff} \propto R^2$, and observe that the dynamics of eq 7 are dominated by $N_{surf}(t)$, we can write

$$I_{sca}(R) \approx R^2 + \alpha N_{surf} \quad (8)$$

Then, from the long-term temporal variability of the flux density $i_{sca} = I_{sca}/R^2$, we should be able to grasp the main trends of the evolution of the surface NPs' number density: $n_{surf} \propto i_{sca}$. As can be seen in Figure 8, the n_{surf} evolution obtained with eq 3 is in very good agreement with i_{sca} obtained from the experiment.

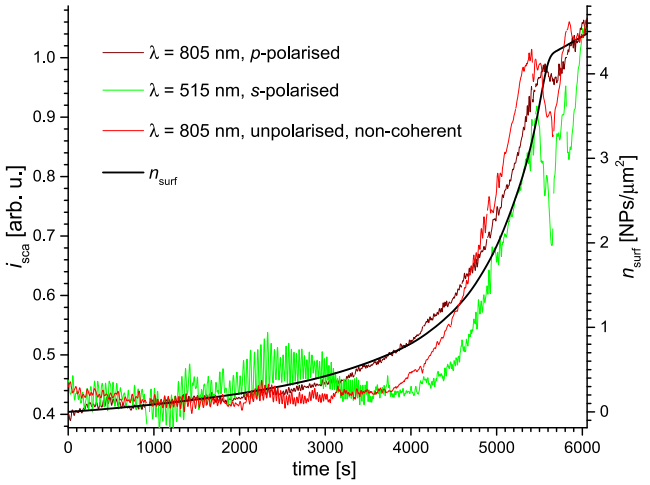

Figure 8. Scattered light flux density at three wavelengths and the modeled surface number density of NPs. The i_{sca} scales at different wavelengths are independent.

It must be kept in mind that the undulations of the optical signals in Figure 8 arise primarily due to specific interactions of light with the NP structure/distribution (surface-thermodynamic states),[40,41] rather than significant short-time variations of n_{surf}. Perhaps with the exception of the collapse(s) of the NP surface layer observed in Figure 8 as deep oscillations near the end of the evolution. It can be further noticed that different wavelengths—different field modes—interact differently with the microdroplet with evolving NP distribution. For instance, it can be observed that the effectiveness of scattering of the noncoherent, unpolarized (red) light from an LED $i_s(632)$ exhibits fairly little interaction with NPs until ~3600 s, when the number of NPs at the droplet surface starts to grow. The $i_s(805)$ of IR coherent light, which is absorbed by NPs (manifesting as smaller modulation depth), seems to detect NPs somewhat deeper below the droplet surface, and thus its increase starts earlier—practically from the beginning. Finally, $i_s(515)$—nonabsorbed, coherent light—additionally shows some interaction with the transient NP structures forming in the microdroplet. This can be seen both as a broad maximum (or maxima) as well as high modulation depth.

3.4.3. Oscillatory Components of Scattering and Luminescence Signals and Their Interpretation. However, the factors discussed so far are not by themselves sufficient to explain the properties of the oscillatory part of the signals. Among others: (i) There are striking transitions from signals (at different wavelengths) oscillating at individual frequencies to synchronized oscillations with a common frequency—see e.g., the transition around 2050 s in the top panel of Figure 9. This synchronicity is lost at ~3500 s. Synchronization repeats at ~4600 s and lasts only until ~4900 s. Initially, the

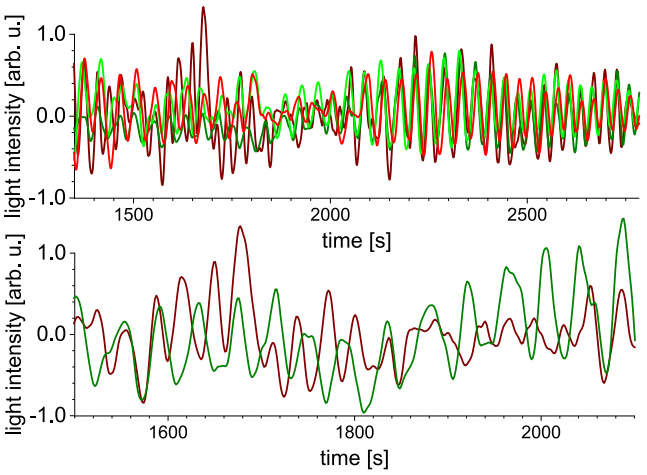

Figure 9. Top panel: transition from signals oscillating at individual frequency to synchronized oscillations with a common frequency, occurring around 2050 s. Bottom panel: out-off-sync scattering at 805 nm, and luminescence at 562 nm, up-converted from 805 nm.

modulation corresponds to spherical cavity modes specific to each wavelength, characterized versus R by a period of $1/\Omega_R = m/4\pi^2\lambda$—as shown in the magnified view in the bottom panel of Figure 9. Over time, this transitions into a single period corresponding to the 805 nm line. This phenomenon seems to be associated with the formation and decay of some regular NP structures at the droplet surface (compare ref 42). (ii) The mean frequency of all signals decreases much more slowly than predicted by the first term of eq 7 alone (effective homogeneous droplet)—compare the violet line with the other lines in Figure 11.

Again, several hypotheses were tested, and as mentioned in Section 3.3, the migration/ordering of NPs caused by intracavity 805 nm radiation was proposed as the common factor influencing both scattering and luminescence across all spectral lines. Thus, it seemed justified to introduce N_{surf} modulation with I_{eff} (λ = 805 nm), as resonances observed in the internal and scattered fields are very similar, as discussed earlier. Furthermore, since it can be well expected that the migration of NPs introduces some lag with respect to the driving radiation intensity due to viscosity, some retardation had to be introduced into the second term. We found that it is proportional to N_{surf}^2, which seems to indicate dependence on the NPs' surface lattice stiffness (NPs' mutual interactions). The interference of the two terms generates beating, which can also be identified in the experimental data, as can be seen in Figure 10. Since the specific resonance features of the system for each wavelength are neglected, the reproduced beating shows only a general property.

The oscillatory part of the signals can be conveniently studied when the slow trend is subtracted from the raw signal, and—in the case of experimental data—some smoothing is performed, which filters out the random fast component of the signal (see Figure 10). This fast-changing component could not be further resolved in the reported experiment (as mentioned in Section 2) due to sensitivity limitations of the spectrometer. Thus, due to possible aliasing, it could not be decided whether deformations and movements of the droplet caused by the trapping field are reflected in this random signal component or are just caused by random inhomogeneity of the microdroplet.

https://doi.org/10.1021/acs.jpcc.5c00174
J. Phys. Chem. C 2025, 129, 8955−8965

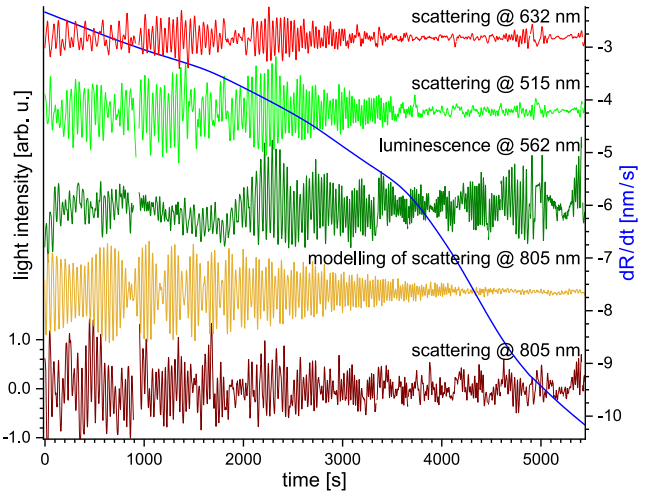

Figure 10. Oscillatory part of optical signals (see main text for details) shown with independent scales. Microdroplet radius change rate is shown as a blue solid line. The orange line corresponds to the first term of eq 7 only.

It can be noticed that "kinks" observed in the evaporation rate dR/dt in Figure 3 seem to closely correlate with rapid changes in the character of oscillations observed in the optical signals in Figure 10. At the same time, it can be observed that as the evaporation rate increases, the frequency of oscillations observed in the optical signals (scattering and luminescence) also increases, as can be generally expected.

In the next step, the extrema (e.g., maxima) in this processed signal, presented in Figure 10, can be identified, and/or frequency analysis (short-time Fourier and wavelet) can be performed. We have decided that analysis of maxima positions presents a convincing visualization of the observed phenomena—see Figure 11. Whenever the traces in such a representation are parallel, the frequencies of signal modulations are identical. The moments when the traces diverge or the slope of the trace changes rapidly mark the dephasing of signal modulation—structural changes are at play in the droplet. There are several such moments, in particular at ∼1000, ∼3500, and ∼4000 s. At ∼2050 s, the general slope/

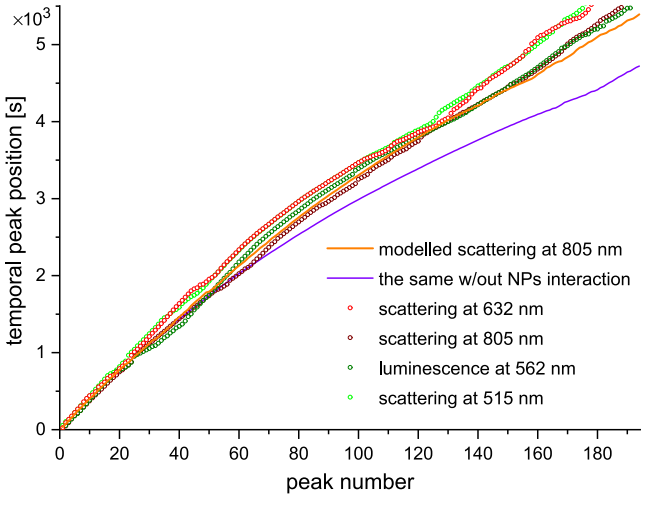

Figure 11. Temporal positions of successive peaks are seen in Figure 10. Color coding corresponds to that figure. The violet solid line represents the prediction based on the first term of eq 7 only.

curvature of the traces changes. Again, these moments correspond to characteristic points (inflection points and "kinks") observed in dR/dt in Figure 3a.

It can also be observed in Figure 11 that the oscillation frequencies of 805 nm scattering (and thus of the internal field) and 562 nm luminescence are nearly identical. This behavior is also replicated in other luminescence signals. The evolution of this oscillation frequency is well reproduced in eq 7, as shown by the orange solid line in Figure 11. As mentioned above, the violet line in Figure 11 corresponds to the first term of this equation only—compare with the orange lines in Figures 7 and 10—confirming that an effective medium description is insufficient in the case of structured microdroplets.

The oscillations of 632 nm scattering of unpolarized noncoherent light from an LED and scattering of 515 nm coherent p-polarized 515 nm laser light are again nearly similar, and both are quite similar to 805 nm field oscillations. It should be kept in mind that 805 nm radiation is absorbed in NPs, while other wavelengths considered in the presented experiments are not. It can also be observed in Figure 10 that each of the presented signals exhibits somewhat different modulation, which signifies different interactions with the inhomogeneous spherical optical cavity − NPs distribution and the microdroplet as a whole. Its evolving structure of MDRs is "scanned" with light of different wavelengths.

At this point, we can summarize our observations and propose a likely scenario for the evolution of the nanoparticle (NP) distribution. Until ∼1000 s, the NPs are randomly dispersed both within the droplet volume and on its surface. Their number concentration increases steadily, leading to a rise in the rate of change of the droplet radius, dR/dt, as a result of increased heating. Although the influence of photophoretic forces is still weak at this stage, it appears sufficient to introduce temporal modulation of the cavity mode structure, resulting in signal oscillations at similar—but not fully synchronized—frequencies.

Around 1000 s, the surface number concentration and/or the average distance between NPs become sufficient to noticeably affect the structure of cavity modes observed at different wavelengths. At this point, an effective medium description becomes inadequate.

At approximately 2050 s, we observe synchronization in the signal oscillations, likely driven by photophoretic forces. This appears to indicate the formation of a regular NP structure at the surface, enhancing radiation absorption and further increasing dR/dt. However, around 3500 s, this synchronization is lost—suggesting that the regular NP structure collapses due to ongoing evaporation. As a result, the process appears to restart at around 4000 s, with a new ordered arrangement emerging by approximately 4600 s.

When the NP concentration approaches its maximum—as the droplet becomes nearly dry—at around 4900 s, the NP organization changes again, likely due to the breakdown of spherical symmetry.

Here, it is worth noting, as a side remark, that the light at 805 nm (the excitation radiation) interacts with light at other wavelengths by modifying the medium (i.e., the distribution of nanoparticles). Under such conditions, the microdroplet can be perceived as optically nonlinear, enabling light−light interaction.

3.5. Long-Term Trend in Luminescence Intensity. The intensity of luminescence (up-conversion) appears easier to

https://doi.org/10.1021/acs.jpcc.5c00174
J. Phys. Chem. C 2025, 129, 8955−8965

analyze than scattering, although the two remain closely related. Luminescence primarily depends on the intensity of the excitation light (at 805 nm) and its correlation with the NP distribution:

$$I_{\text{lumi}} \sim \int_0^{2\pi R} N(x) I^2(\lambda = 805\,\text{nm}, x)\,\mathrm{d}x \tag{9}$$

It can be divided into two components: one that is proportional to the number of illuminated nanoparticles and an oscillatory component that reflects how well the excitation radiation spherical cavity (droplet) mode aligns with the mean distance between the NPs. Since luminescence is driven by 805 nm intracavity radiation, it also inherits the oscillatory properties predicted with eq 7. The long-term signal variation requires additional consideration. It should also be kept in mind that for the up-conversion-driven luminescence, $I_{\text{lumi}} \propto I_0^2$, where I_0 is the incident light intensity.

Under the reasonable assumption that the quantum efficiency of Er^{3+} luminescence in the Gd_2O_3 lattice can be considered constant, the luminescence signal must depend directly on the number of excited Er^{3+} ions. Since the concentration of Er in Gd_2O_3 is constant for a given sample, the luminescence signal I_{lumi} must then depend linearly on the (total) number of NPs N_{tot}. Since we are considering a long-term trend, it is sufficient to consider that the energy of the 805 nm radiation that can be passed to Er^{3+} is proportional to the geometric cross-section of the microdroplet. While N_{tot} is obviously constant, the cross-section of the microdroplet evolves over time as $R^2(t)$.

However, these considerations do not explain the broad maximum observed in the luminescence signals, which exactly overlaps with all luminescence spectral lines. This maximum seems to signify some resonant features of the system. Furthermore, the resonance must be attributed to a single wavelength, as there is no temporal shift between signals at different wavelengths. It can be well expected that, once again, it must be attributed to 805 nm radiation (excitation). In line with our previous works,[40,43] we expect that the distributed feedback/additional resonance introduced by the specific NP distribution strongly enhances two-photon excitation (up-conversion). This effect cannot be identified in scattering, which is dominated by scattering on the droplet as a whole, while it is also a single-photon process.

Thus, it makes sense to compare the mean distance between NPs with the wavelength and the distance between field maxima and minima on the cavity circumference. Here, comparing the distribution of NPs described by eq. 2) with the excitation radiation wavelength in the (effective) medium, λ, yielded the expected results. Thus, the intensity of luminescence could be approximated as

$$I_{\text{lumi}} = aR^2 N_{\text{tot}} + b\frac{N_{\text{surf}}}{\sigma\sqrt{2\pi}}\exp\left(-\left(\frac{x(R) - \lambda}{\sqrt{2}\,\sigma}\right)^2\right) \tag{10}$$

where, a and b are constants. We confirmed with the fit—see Figure 12—that N_{surf} must be, in a way, accounted for twice: the first term must contain N_{tot}, rather than the number of NPs only below the surface: $N_{\text{tot}} - N_{\text{surf}}$, and the second term accounts for an additional resonant feature.

It can be observed that the peak value of the resonance maximum in the luminescence signal depends on the width of the particle distribution, σ. A similar effect manifests in the interaction of the light field with a regularly structured NP

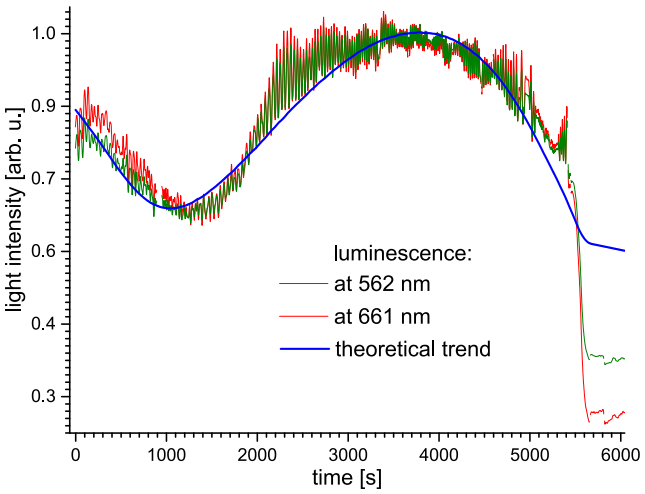

Figure 12. Luminescence at two spectra lines resulting from different up-conversion mechanisms, together with the prediction with eq 10.

distribution. This can be observed at ~2050 s and ~4600 s in Figure 10 as an increase in the luminescence modulation amplitude. Therefore, the amplitude of luminescence intensity modulation could serve as a measure of σ.

Notably, in the language of surface thermodynamics, the width of the particle distribution, σ, is related to the entropy of the particle layer at the surface (see, e.g ref 44:

$$H = \frac{1}{2}\log(2\pi\sigma^2) + \frac{1}{2} \tag{11}$$

This connection should allow us to quantify the disorder or randomness of the particle arrangement on the surface by measuring the amplitude of the luminescence signal modulation.

4. CONCLUSION

This study explores the dynamic optical properties of single evaporating microdroplets containing up-converting luminescent nanoparticles (Gd_2O_3:Er^{3+}). Acting as spherical optical cavities, these microdroplets enable detailed investigation of the interplay between light−matter interactions, resonance phenomena, and evolving nanoparticle distributions.

Resonant modes within the droplets, particularly whispering gallery modes, form standing wave patterns that dynamically interact with the spatial arrangement of nanoparticles, modulating both scattered and luminescent light intensities. Deviations from perfect symmetry—caused by nanoparticle inclusions or surface irregularities—break the degeneracies of these modes and significantly influence the optical response (compare ref 45).

As evaporation progresses, nanoparticles become increasingly concentrated (primarily) at the droplet surface, leading to distinct stages of surface evolution (compare refs 10,11) (i) a uniform distribution of suspended nanoparticles (also on the surface), (ii) a surface covered by an irregular nanoparticle film, and (iii) a surface exhibiting a regular, ordered nanoparticle film. Each of these surface states affects the resonance behavior in specific ways, altering the mode intensities, spectral positions, and their temporal evolution.

Photophoretic forces, induced by the strong internal excitation field (at 805 nm), contribute to nanoparticle redistribution by driving them toward the intensity minima

https://doi.org/10.1021/acs.jpcc.5c00174
J. Phys. Chem. C 2025, 129, 8955−8965

within the droplet. This enhances the structural complexity at the surface and influences the observed resonance dynamics.

Theoretical modeling aligns well with experimental observations, confirming that the evolving nanoparticle distribution plays a crucial role in shaping the droplet's optical properties. The interplay between droplet evaporation, surface transformation, and resonance behavior provides deeper insight into light−matter interactions in colloidal systems.

These findings have broader implications for understanding aerosol dynamics, nanoparticle self-assembly, and evaporation-driven transformations in microdroplets. Further investigation into multicomponent droplet systems could yield valuable insights into the physicochemical processes governing such complex optical behaviors.

AUTHOR INFORMATION

Corresponding Author

Daniel Jakubczyk − *Institute of Physics, Polish Academy of Sciences, Warsaw 02-668, Poland;* orcid.org/0000-0002-2144-3228; Email: jakub@ifpan.edu.pl

Authors

Yaroslav Shopa − *Cardinal Stefan Wyszynski University in Warsaw, Warsaw 01-815, Poland*

Maciej Kolwas − *Institute of Physics, Polish Academy of Sciences, Warsaw 02-668, Poland*

Gennadiy Derkachov − *Institute of Physics, Polish Academy of Sciences, Warsaw 02-668, Poland*

Izabela Kamińska − *Institute of Physics, Polish Academy of Sciences, Warsaw 02-668, Poland*

Krzysztof Fronc − *Institute of Physics, Polish Academy of Sciences, Warsaw 02-668, Poland; International Research Centre MagTop, Warsaw 02-668, Poland*

Tomasz Wojciechowski − *Institute of Physics, Polish Academy of Sciences, Warsaw 02-668, Poland; International Research Centre MagTop, Warsaw 02-668, Poland*

Complete contact information is available at: https://pubs.acs.org/10.1021/acs.jpcc.5c00174

Notes

The authors declare no competing financial interest.

ACKNOWLEDGMENTS

This research was funded in whole or in part by the National Science Centre, Poland, grant 2021/41/B/ST3/00069. For the purpose of Open Access, the author has applied a CC-BY public copyright license to any Author Accepted Manuscript (AAM) version arising from this submission. During the preparation of this work, the authors used ChatGPT 4o in order to interactively compose the Abstract and Conclusion, and to improve the style of several paragraphs in other sections. After using this tool/service, the authors reviewed and edited the content as needed and take full responsibility for the content of the published article.

REFERENCES

(1) *Optical Properties of Nanostructured Random Media*. Topics in Applied Physics. Shalaev, V. M.. ed.; Springer; 2002. Vol. *82*.

(2) Iannacchione, G.; Pal, A.Bio-Colloidal Drying Droplets: Current Trends and Future Perspectives on Image Processing Applications*Acad. Lett.***2021***2*

(3) Arakawa, A.; Jung, J. H.; Wu, C. M. Toward Unification of the Multiscale Modeling of the Atmosphere. *Atmos. Chem. Phys.* **2011**, *11* (8), 3731−3742.

(4) Tao, W. K.; Moncrieff, M. W. Multiscale Cloud System Modeling. *Rev. Geophys.* **2009**, *47* (3), 1−41.

(5) Zang, D.; Tarafdar, S.; Tarasevich, Y. Y.; Dutta Choudhury, M.; Dutta, T. Evaporation of a Droplet: From Physics to Applications. *Phys. Rep.* **2019**, *804*, 1−56.

(6) Diveky, M. E.; Roy, S.; Cremer, J. W.; David, G.; Signorell, R. Assessing Relative Humidity Dependent Photoacoustics to Retrieve Mass Accommodation Coefficients of Single Optically Trapped Aerosol Particles. *Phys. Chem. Chem. Phys.* **2019**, *21* (9), 4721−4731.

(7) Parviz, B. A.; Ryan, D.; Whitesides, G. M. Using Self-Assembly for the Fabrication of Nano-Scale Electronic and Photonic Devices. *IEEE Trans. Adv. Packag.* **2003**, *26* (3), 233−241.

(8) Symes, R.; Sayer, R. M.; Reid, J. P. Cavity Enhanced Droplet Spectroscopy: Principles Perspectives And Prospects. *Phys. Chem. Chem. Phys.* **2004**, *6* (3), 474.

(9) Cai, L.; Pan, J.; Zhao, Y.; Wang, J.; Xiao, S. Whispering Gallery Mode Optical Microresonators: Structures and Sensing Applications. *Phys. Status Solidi Appl. Mater. Sci.* **2020**, *217* (6), 1−18.

(10) Jakubczyk, D.; Kolwas, M.; Derkachov, G.; Kolwas, K. Surface States of Microdroplet of Suspension. *J. Phys. Chem. C* **2009**, *113* (24), 10598−10602.

(11) Kolwas, M.; Kolwas, K.; Derkachov, G.; Jakubczyk, D. Surface Diagnostics of Evaporating Droplets of Nanosphere Suspension: Fano Interference and Surface Pressure. *Phys. Chem. Chem. Phys.* **2015**, *17* (10), 6881−6888.

(12) Chang, S.; Eichmann, S. L.; Huang, T. Y. S.; Yun, W.; Wang, W. Controlled Design and Fabrication of SERS-SEF Multifunctional Nanoparticles for Nanoprobe Applications: Morphology-Dependent SERS Phenomena. *J. Phys. Chem. C* **2017**, *121* (14), 8070−8076.

(13) Sreejith, S.; Ajayan, J.; Radhika, J. M.; Uma Reddy, N. V.; Manikandan, M. Recent Advances in Nano Biosensors: An Overview. *Measurement* **2024**, *236* (March), 115073.

(14) Shopa, Y.; Kolwas, M.; Kamińska, I.; Derkachov, G.; Nyandey, K.; Jakubczyk, T.; Wojciechowski, T.; Derkachova, A.; Jakubczyk, D. Luminescent Nanoparticles in a Shrinking Spherical Cavity − Probing the Evaporating Microdroplets of Colloidal Suspension − Optical Lattices and Structural Transitions. *J. Quant. Spectrosc. Radiat. Transfer.* **2023**, *296*, 108439.

(15) Lohmann, U.; Friebel, F.; Kanji, Z. A.; Mahrt, F.; Mensah, A. A.; Neubauer, D. Future Warming Exacerbated by Aged-Soot Effect on Cloud Formation. *Nat. Geosci.* **2020**, *13* (10), 674−680.

(16) Li, Z.; Lau, W. K.-M.; Ramanathan, V.; Wu, G.; Ding, Y.; Manoj, M. G.; Liu, J.; Qian, Y.; Li, J.; Zhou, T. Aerosol and Monsoon Climate Interactions over Asia. *Rev. Geophys.* **2016**, *54* (4), 866−929.

(17) Rezaei, M.; Netz, R. R. Airborne Virus Transmission via Respiratory Droplets: Effects of Droplet Evaporation and Sedimentation. *Curr. Opin. Colloid Interface Sci.* **2021**, *55*, 101471.

(18) Woźniak, M.; Archer, J.; Wojciechowski, T.; Derkachov, G.; Jakubczyk, T.; Kolwas, K.; Kolwas, M.; Jakubczyk, D. Application of a Linear Electrodynamic Quadrupole Trap for Production of Nanoparticle Aggregates from Drying Microdroplets of Colloidal Suspension. *J. Instrum* **2019**, *14* (12), 12007−P12007.

(19) Davis, E. J. A History of Single Aerosol Particle Levitation. *Aerosol Sci. Technol* **1997**, *26* (3), 212−254.

(20) Hart, M. B.; Sivaprakasam, V.; Eversole, J. D.; Johnson, L. J.; Czege, J. Optical Measurements from Single Levitated Particles Using a Linear Electrodynamic Quadrupole Trap. *Appl. Opt.* **2015**, *54* (31), F174.

(21) Kamińska, I.; Elbaum, D.; Sikora, B.; Kowalik, P.; Mikulski, J.; Felcyn, Z.; Samol, P.; Wojciechowski, T.; Minikayev, R.; Paszkowicz, W. Single-Step Synthesis of Er3+ and Yb3+ Ions Doped Molybdate/Gd2 O3 Core−Shell Nanoparticles for Biomedical Imaging. *Nanotechnology* **2018**, *29* (2), 025702.

(22) Riefler, N.; Wriedt, T.; Fritsching, U. Flexible Piezoelectric Drop-On-Demand Droplet Generation. In *Proceedings ILASS−Europe*

2017. 28th Conference on Liquid Atomization and Spray Systems; Universitat Politècnica: València, 2017. .
(23) Shopa, Y.; Kolwas, M.; Jakubczyk, D.; Derkachov, G.; Kamińska, I.; Fronc, K.; Wojciechowski, T. Evaporation of levitating microdroplets containing nanoparticles: Luminescent Gd2O3: Er3+, illumination with 806 nm laser from below via optical fiber. *Mendeley Data*. .
(24) Jakubczyk, D.; Kolwas, M.; Derkachov, G.; Kolwas, K.; Zientara, M. Evaporation of Micro-Droplets: The "Radius-Square-Law. *Revisited. Acta Phys. Polym. A* **2012**, *122* (4), 709−716.
(25) Derkachov, G.; Jakubczyk, D.; Woźniak, M.; Archer, J.; Kolwas, M. High-Precision Temperature Determination of Evaporating Light-Absorbing and Non-Light-Absorbing Droplets. *J. Phys. Chem. B* **2014**, *118* (43), 12566−12574.
(26) Sirignano, W. A. *Fluid Dynamics and Transport of Droplets and Sprays, Second Edi.*; 2nd; Cambridge University Press; 2010.
(27) Pruppacher, H. R.; Klett, J. D. *Microphysics of Clouds and Precipitation*; Atmospheric and Oceanographic Sciences Library; Springer Dordrecht; 2010; Vol. *18*.
(28) Woźniak, M.; Derkachov, G.; Kolwas, K.; Archer, J.; Wojciechowski, T.; Jakubczyk, D.; Kolwas, M. Formation of Highly Ordered Spherical Aggregates from Drying Microdroplets of Colloidal Suspension. *Langmuir* **2015**, *31* (28), 7860−7868.
(29) Kolwas, M.; Jakubczyk, D.; Archer, J.; Duc, T. D. Evolution of Mass, Surface Layer Composition and Light Scattering of Evaporating, Single Microdropletes of SDS/DEG Suspension. Shrinking Droplet Surface as the Micelles Generator. *J. Quant. Spectrosc. Radiat. Transfer.* **2021**, *258*, 107396.
(30) Bohren, C. F.; Huffman, D. R. *Absorption and Scattering of Light by Small Particles*; Wiley, 1998. .
(31) Sorensen, C. M. Light Scattering by Fractal Aggregates: A Review. *Aerosol Sci. Technol.* **2001**, *35* (2), 648−687.
(32) Tzarouchis, D.; Sihvola, A. Light Scattering by a Dielectric Sphere: Perspectives on the Mie Resonances. *Appl. Sci.* **2018**, *8* (2), 184.
(33) Mätzler, C.*MATLAB Functions for Mie Scattering and Absorption*Institut für Angewandte Physik2002
(34) Chýlek, P.; Pendleton, J. D.; Pinnick, R. G. Internal and Near-Surface Scattered Field of a Spherical Particle at Resonant Conditions. *Appl. Opt* **1985**, *24* (23), 3940.
(35) Machfuudzoh, I.; Hinamoto, T.; García de Abajo, F. J.; Sugimoto, H.; Fujii, M.; Sannomiya, T. Visualizing the Nanoscopic Field Distribution of Whispering-Gallery Modes in a Dielectric Sphere by Cathodoluminescence. *ACS Photonics* **2023**, *10* (5), 1434−1445.
(36) Arnold, S.; Ramjit, R.; Keng, D.; Kolchenko, V.; Teraoka, I. MicroParticle Photophysics Illuminates Viral Bio-Sensing. *Faraday Discuss* **2008**, *137*, 65−83.
(37) Dong, L.; Johnson, D. Surface Tension of Charge-Stabilized Colloidal Suspensions at the Water−Air Interface. *Langmuir* **2003**, *19* (24), 10205−10209.
(38) Ngo, D.; Pinnick, R. G. Suppression of Scattering Resonances in Inhomogeneous Microdroplets. *J. Opt. Soc. Am. A* **1994**, *11* (4), 1352.
(39) Gobel, G.; Lippek, A.; Wriedt, T.; Bauckhage, K. Monte Carlo Simulation of Light Scattering by Inhomogeneous Spheres. In *Proceedings of the Second International Symposium on Radiation Transfer*; Connecticut: Begellhouse, 1997, pp. 1−10. .
(40) Kolwas, M.; Jakubczyk, D.; Derkachov, G.; Kolwas, K. Interaction of Optical Whispering Gallery Modes with the Surface Layer of Evaporating Droplet of Suspension. *J. Quant. Spectrosc. Radiat. Transfer.* **2013**, *131*, 138−145.
(41) Jakubczyk, D.; Derkachov, G.; Bazhan, W.; Łusakowska, E.; Kolwas, K.; Kolwas, M. Study of Microscopic Properties of Water Fullerene Suspensions by Means of Resonant Light Scattering Analysis. *J. Phys. D: appl. Phys.* **2004**, *37* (20), 2918−2924.
(42) Archer, J.; Kolwas, M.; Woźniak, M.; Jakubczyk, D.; Kolwas, K.; Derkachov, G.; Wojciechowski, T. Sodium Dodecyl Sulfate Micro-aggregates with Diversely Developed Surfaces: Formation from Free Microdroplets of Colloidal Suspension. *Eur. Phys. J. Plus.* **2019**, *134* (1), 39.
(43) Kolwas, M.; Kolwas, K.; Jakubczyk, D.; Derkachov, G. Collective Scattering of Light on Gold Nanospheres Dispersed in Diethylene Glycol Microdroplet. *Acta Phys. Pol., A* **2017**, *131* (1), 288−293.
(44) Lazo, A. V.; Rathie, P. On the Entropy of Continuous Probability Distributions (Corresp.). *IEEE Trans. Inf. Theory* **1978**, *24* (1), 120−122.
(45) Kher-Alden, J.; Maayani, S.; Martin, L. L.; Douvidzon, M.; Deych, L.; Carmon, T. Microspheres with Atomic-Scale Tolerances Generate Hyperdegeneracy. *Phys. Rev. X* **2020**, *10* (3), 031049.

https://doi.org/10.1021/acs.jpcc.5c00174
J. Phys. Chem. C 2025, 129, 8955−8965